Sustainable Structure and Materials, *Vol. 1, No .2, (2018) 54-72*
DOI: https://doi.org/10.26392/SSM.2018.01.02.054

Compressive Strength Variability in High Performance Concrete with Steel Fiber Addition

Abdulhameed Umar Abubakar*

Civil Engineering Department, Modibbo Adama University of Technology, Yola, Nigeria
*Corresponding E-mail: abdulhameed.umar@mautech.edu.ng

(Received: October 07, 2018, Revised: November 19, 2018, Accepted: December 11, 2018)

ABSTRACT. *In this study, an evaluation was conducted on the influence of specimen geometry on high performance concrete (HPC) with steel fiber addition with a view of monitoring the variability that exists. Strict mix design protocols were carried out in the production of the HPC based on the relevant standard, and strict procedures were ensured in the casting, consolidation, and curing of the specimens to produce viable specimens for testing. Standard 150 x 300 mm cylinder and 150 mm side cubes were utilized. There is an observed strength increase for both type of specimens and aspect ratios, as well as a noticeable wall effect especially in the cylindrical specimens at higher aspect ratio of fiber. Variability of the results is more prominent in lower aspect ratio of the fiber irrespective of the specimen type due to data range. At the end, due to strict quality control, the range of the data has been successfully reduced to about 2-3 MPa in most cases.*

Keywords: High performance concrete, steel fiber-reinforced concrete, compressive strength variability, cylinder-to-cube ratio, mean strength, standard deviation.

1. INTRODUCTION

The initiation of vertical cracking in concrete specimen subjected to uniaxial compression starts at a load equal to or 50 – 70 % of the ultimate load, and this largely depends on the properties of the coarse aggregate [1]. This ultimate load point depends on the property of the material at a point very close to the onset of crack propagation, where in high performance concretes (HPC) is a very narrow region before failure. In Abubakar [2], this point is reported to be around 85 – 91% of the ultimate load in HPC with steel fiber addition. These concretes are engineered to possess higher toughness and lower brittleness, with improved cracking resistance and better durability [3].

It has been established that one view point regarding the failure of concrete under compression is that of Newman's [4] discontinuity stress point, which correspond to instability of the matrix and beyond failure occurs. In here, lateral tensile strain is relay on the level of compressive loading, which tends to be higher as the strength class of concrete increase [1]. That is why failure under uniaxial compression is either tensile failure of cement crystals, bond in the direction perpendicular to the applied load, or collapse by development of inclined shear planes [5]. In Van Mier [6] cited in del Viso et al. [7] reported that from experimental investigation, failure pattern results from a localized microcracked area that develops at peak stress or prior. Hence, the reason why the analysis of compressive failure by fracture mechanics is the most ideal [8]. Therefore, the application of this important parameter in strength determination cannot be overemphasized, and the most widely used dimensions in compressive strength testing are 150 x 300 mm cylinders and 100 mm and 300 mm cubic dimensions. The former used mostly in North America, while the latter in Europe. However, the use of these different dimensions comes with variations when the cylinder-cube ratio is compared.

The work of Tam et al. [9] attributed this difference in the measured strength between the cylinder and cube to the difference in the aspect ratio in relation to the restraining effect by the steel platen of the testing machine on the lateral expansion of the concrete in the parts of the specimen near its ends. On the other hand, in the cylinders, volumetric expansion occurs in the middle of the specimen prior to ultimate load. In the case of the cube, there is an overlapping of the affected zones, but for a cylindrical specimen with l/d ratio of 2.0, there is a middle zone free of this influence. Hence, the measured strength of a standard cylinder specimen is lower than that of a standard cube specimen of the same lateral dimension.

A series of investigations by Hamad [10] reported on the size and shape effect on cube and cylinder in high performance lightweight foamed concrete reinforced with glass fiber that there is a disparity in compressive strength for two sizes and shapes measured. However, it reduces with increase in volume fraction of glass fibers. Also, Nakbin et al. [11] reported a lower strength ratio in self-compacting concrete (SCC) specimens (0.749) in comparison with normal strength concrete (NSC).

It has been reported by Juki et al. [12] that this ratio for a specimen of constant length-diameter (l/d) of 2.0 to be between 0.74 – 1.16 with an average of 0.91. An earlier work by Tokyay and Ozdemir [13] reported no significant effect for l/d ratio of cylinder specimens on the compressive strength of high strength concrete (HSC).

Fiber orientation is another factor that influences the compressive strength in concrete with fiber addition. In other to be able to utilize steel fibers in structural applications, the dispersion process of fibers has to be properly taken care of [14]. It has been reported by Barnett et al. [15] that the flow direction of fibers tends to be perpendicular to the flow of the concrete. According to Soroushian and Lee [16], the vibration of steel fiber reinforced concrete seems to reorient the fibers towards the horizontal planes. And in an attempt to derive expression for orientation factor, with specimens of width-to-height ratio of 1, 3, and 6, they concluded that it plays an important role in deciding the orientation factor. In Mansur et al. [17], when cylinders and prisms were used to study the effect of specimen shape, it was seen that when casting and testing was done in an upright position, fibers and coarse aggregates predominantly align themselves in a direction perpendicular to the loading axis. The situation is reversed on the other hand when the specimens are casted horizontally but tested in an upright position.

In general, according to Afroughsabet et al. [18] fiber orientation is affected by properties in the fresh state, casting method, vibration, flow direction, and wall effect [19-22]. This is to say that fiber alignment has a considerable influence on mechanical properties of fibered concrete. These developments have led to innovative ideas such as the utilization of staplewire fiber reinforced concretes with encouraging results [23].

It is on this premise that a study utilizing HPC with steel fiber addition is important, though there are many numerous studies in lower strength class, but the uniqueness of this will further gives us insight in the future into the fracture process of HPC at ‘discontinuity’ stress region.

2. EXPERIMENTAL PROCEDURE

Blast-furnace Slag Cement CEM II/B-S 42.5 N in conformity with ASTM C 595 [24] was utilized with a specific gravity of 3.15; silica fume was added at 10% of the cement content with 82 % content of SiO_2, and tap water utilized conformed with BS EN 1008 [25]. High range water reducer (HRWR) utilized was GLENIUM 27 conforming with ASTM C 494 [26] ether basis brown in color with a density of 1,023 – 1,063 kg/lt color content <0.1 % and alkali content <3%.

Table-1: Mix design utilized for HPC

Material	Cement 42.5 N(Slag)	Water	Coarse (10mm max)	Fine (5mm max)	Silica Fume	HRWR
Quantity (kg/m^3)	470	165	1050	700	47	14

Aggregates used were crushed limestone rock conforming to the specification of ASTM C 33 [27] and sieve analysis was conducted in accordance with ASTM C 136 [28] and the result presented.

Table-2: Sieve analysis of aggregates

Sieve sizes (mm)	12.5	9.5	4.75	2.36	1.18	0.6	0.3	0.15	0.075
% passing coarse	100	100	9.4	0.2	0.2	-	-	-	-
% passing fine	-	-	100	82	48	29	17	7	3

Relative density (SSD) performed for both fine and coarse aggregates were based on ASTM C 127 [29] and ASTM C 128 [30] and were 2.68 and 2.65 respectively, also absorption (%) determined based on the same standards were 3.0 % and 0.7 %. Bulk density was based on ASTM C 29 [31] were 2083 kg/m^3 and 1203 kg/m^3. Voids in aggregates were 25 % and 50 % respectively for fine and coarse aggregates. The percentage of materials finer than 75µm to ASTM C117 [32] was 3%. Hooked end steel fiber were utilized with the following volume fractions 0.5, 0.75, 1.0, 1.25, 1.50, 1.75, & 2.00 % by volume of concrete (39.25, 58.88, 78.50, 98.125, 117.75, 137.38 & 157.01 kg/m^3, respectively). Steel fibers conformed to ASTM A820 [33] with the properties presented in Table 3.

Table-3: Dimensions and tensile strength of steel fibers

Length (mm)	Diameter (mm)	L/d Ratio	Tensile Strength (MPa)
30	0.50	60	1250
60	0.80	75	1100

Mixing operation was done as prescribed by the manufacturer with the fibers which are stacked in a fibrillated bundle of water soluble glue placed last by distribution in small amount to avoid balling. Immediately upon contact with moisture they were dispersed but the mixing time was relatively longer for volume percentages from 1.25 % and above.

Concrete compressive strength was tested at age of 28 days in accordance with ASTM C39 [34] using 150 x 300 mm cylinders at a loading rate of 0.5 MPa/s. In comparison, prismatic specimens when tested based on BS EN 12390 – 3 [35] with 150 mm cubic prisms at the same loading rate on a 3,000 kN capacity machine. Splitting tensile strength of concrete (Brazilian Test) was done to BS EN 12390 – 6 [36] on 150 mm cubic prisms dimension with a loading rate of 0.4 kN/s. Minitab 18 [37] statistical software which can be obtained freely on the web was used in some portion for the analysis of the result.

3. RESULTS & DISCUSSION

3.1 Strength Properties

It has been highlighted already that the ultimate strength of concrete depends on the behavior at the region that is very close to the failure load, where there is rapid propagation of multiple cracks from micro to macro by coalescing together, and these cracks moves parallel to the direction of the loading. In concrete with fiber addition, at this point the fibers that are in the direction of these cracks intercept the cracks, which results in the high carrying capacity of the composite. However, if the fibers are aligned in the direction of the cracks, the crack will progress parallel to the fiber, and little resistance to the crack growth will be offered. This

mostly occur in cylindrically casted specimens (Fig. 1a and section in Fig. 1b) where the fibers align themselves in vertical direction parallel to the direction of the casting. On the other hand, in prismatic specimens, fibers align themselves horizontally during vibration due to 'wall' effect and restrain provided by the boundary. This conforms to what has been reported by [15-17, 38].

In Table 4-5 Figure 2-3, the strength results in compression for the specimens incorporated with fibers at aspect ratio 60 and 75 respectively for cubic and cylindrical specimens are presented. Results indicates that the strength in aspect ratio 60 increases with volume fractions (V_f) compared with the plain concrete, while in aspect ratio 75, compressive strength increment with V_f was observed up to 1 %, and beyond this point it decreased in a fluctuating manner. Results obtained in aspect ratio 75 were still better than the reference sample despite the decline in the values, but the aspect ratio 60 results fared better. This has been pointed out by Eren and Celik [39] that the content and aspect ratio govern the compressive strength of the fibered concrete.

The increase in f_c in high strength concretes is due to delayed microcrack formation within the concrete under uniaxial compression. At higher V_f, this effect of fiber bridging is more pronounced especially at lower aspect ratio. There is also the effect of a strong bond between the fiber and matrix interface especially at higher V_f thereby decreasing the distance between fiber to fiber hence improving the strength of the composite.

In Figure 4, relationship between cylinder compressive strength and that of its cubic counterpart is presented. It is seen that due to the fluctuation in the results for aspect ratio 75, the coefficient of determination was quite low. On the other hand, aspect ratio 60 specimens presented a very strong correlation. In Table 6, the ratio of cylindrical compressive strength to the cubic for both aspect ratios is presented, and the values ranged between 0.769 – 0.900. According to Neville [1] cited from Evans [40], that the ratio slightly increases with increase in strength and nearly approaches 1 for concretes with strength above 100 MPa. However, as it was noted, other factors such as moisture condition at time of testing plays crucial role. In CEB-FIP [41] code, ratios up to 0.89 have been suggested for concrete above 50 MPa.

Another observable feature is 'wall effect' that was visible especially in the cylindrical specimens, this is the wall or boundary influences the packing of the constituents' materials especially when larger size coarse aggregates are used. In other to reduce this effect, ASTM C 192 [42] has provided that the diameter of the test cylinder or minimum dimension of a prism be at least 3 times the nominal maximum size of the aggregate. In this study, for both cylinder and prismatic specimens, this requirement has been met, however, fiber addition resulted in this phenomenon, and this was more apparent at higher volume fractions. It was also more dominant in the larger aspect ratio (l/d = 75) specimens because of the amount of fiber per unit area.

Splitting tensile strength was measured using the Brazilian test and the result presented in Table 7. It can be seen that f_{st} showed a slight increment up to 1 % V_f, however beyond that level (from 1 – 2 %), higher rate of increment relative to the reference sample has been observed. In aspect ratio 75 on the other hand, from 0.5 - 1 % V_f values obtained for f_{st} were all lower than the reference sample. This could be attributed to the random orientation of the fibers and their distribution, as well as high amount of coarse aggregate at a lower volume fraction that reduces the efficiency of the fibers in deflecting and bridging the splitting crack. Tensile resistance of steel fiber incorporated in concrete is also responsible, where fibers in the plane of fracture resist the propagation of cracks by progressive pull-out, building up stresses, and therefore increasing f_{st}. In Figures 5-7, relationships have been established with splitting tensile

strength and presented with values of their coefficient of determination. However, in Figure 7, the relationship was established between splitting tensile strength and cubic compressive strength only.

Fig-1: (a) Fibers aligned vertically on the wall of the cylinder (b) A section through the cylindrical specimen showing the cut fiber surface

Table-4: Compressive Strength Results for Cubes

Aspect Ratio 60 Cubic Specimens							
Fiber Volume (%)	**Sample 1**	**Sample 2**	**Sample 3**	**Average**	**Standard Deviation**	**Standard Error**	**Variance**
0.00	79.30	77.40	81.20	79.30	1.90	1.10	3.61
0.50	89.40	92.20	90.40	90.70	1.42	0.82	2.01
0.75	92.20	93.00	91.40	92.20	0.80	0.46	0.64
1.00	100.50	98.00	97.60	98.70	1.57	0.91	2.47
1.25	102.60	99.70	98.90	100.40	1.95	1.13	3.79
1.50	110.40	108.00	108.30	108.90	1.31	0.76	1.71
1.75	107.10	109.20	109.60	108.90	1.34	0.77	1.80
2.00	115.60	117.20	115.00	116.00	1.14	0.66	1.29
Aspect Ratio 75 Cubic Specimens							
Fiber Volume (%)	**Sample 1**	**Sample 2**	**Sample 3**	**Average**	**Standard Deviation**	**Standard Error**	**Variance**
0.50	90.90	92.40	91.80	91.70	0.75	0.43	0.57
0.75	92.90	95.00	93.40	93.80	1.10	0.64	1.20
1.00	98.30	100.90	102.30	100.50	2.03	1.17	4.12
1.25	94.30	94.60	94.20	94.40	0.21	0.12	0.04
1.50	98.00	102.00	100.30	100.10	2.00	1.15	4.03
1.75	108.30	107.00	105.70	107.00	1.30	0.75	1.69
2.00	99.80	98.00	99.20	99.00	0.92	0.53	0.84

Table-5: Compressive Strength Results for Cylinders

Aspect Ratio 60 Cylindrical Specimens							
Fiber Volume (%)	**Sample 1**	**Sample 2**	**Sample 3**	**Average**	**Standard Deviation**	**Standard Error**	**Variance**
0.00	70.90	71.10	71.00	71.00	0.10	0.06	0.01
0.50	72.00	70.30	71.00	71.10	0.85	0.49	0.73
0.75	77.50	76.10	75.30	76.30	1.11	0.64	1.24
1.00	80.00	82.00	80.40	80.80	1.06	0.61	1.12
1.25	81.90	82.90	83.60	82.80	0.85	0.49	0.73
1.50	83.20	83.00	84.90	83.70	1.04	0.60	1.09
1.75	87.80	88.80	88.90	88.50	0.61	0.35	0.37
2.00	92.00	91.80	91.30	91.70	0.36	0.21	0.13
Aspect Ratio 75 Cylindrical Specimens							
Fiber Volume (%)	**Sample 1**	**Sample 2**	**Sample 3**	**Average**	**Standard Deviation**	**Standard Error**	**Variance**
0.50	73.50	73.90	72.80	73.40	0.56	0.32	0.31
0.75	76.00	75.20	76.20	75.80	0.53	0.31	0.28
1.00	77.90	78.40	78.30	78.20	0.26	0.15	0.07
1.25	81.00	82.00	80.00	81.00	1.00	0.58	1.00
1.50	79.70	80.60	80.90	80.40	0.62	0.36	0.39
1.75	83.10	83.70	84.30	83.70	0.60	0.35	0.36
2.00	81.70	82.70	81.90	82.10	0.53	0.31	0.28

Table-6: Splitting Tensile Strength Results

Aspect Ratio 60 f_{st} (MPa)						
Fiber Volume (%)	**Sample 1**	**Sample 2**	**Sample 3**	**Average**	**Standard Deviation**	**Variance**
0.00	4.72	4.95	5.27	4.98	0.28	0.08
0.50	5.75	5.82	5.65	5.74	0.09	0.01
0.75	5.73	5.94	5.79	5.82	0.11	0.01
1.00	6.12	6.35	6.10	6.19	0.14	0.02
1.25	6.50	6.85	6.99	6.78	0.25	0.06
1.50	6.99	7.48	9.35	7.94	1.25	1.55
1.75	8.90	8.72	8.69	8.77	0.11	0.01
2.00	9.08	9.21	8.50	8.93	0.38	0.14
Aspect Ratio 75 f_{st} (MPa)						
Fiber Volume (%)	**Sample 1**	**Sample 2**	**Sample 3**	**Average**	**Standard Deviation**	**Variance**
0.50	3.17	3.09	3.67	3.30	0.31	0.10
0.75	3.95	4.33	4.62	4.30	0.34	0.11
1.00	4.99	4.70	4.71	4.80	0.16	0.03
1.25	5.48	5.31	5.11	5.30	0.19	0.03
1.50	7.14	6.98	6.88	7.00	0.13	0.02
1.75	10.12	10.10	10.08	10.10	0.02	0.00
2.00	11.64	12.65	11.65	11.80	0.58	0.34

Table-7: Ratio of Tensile-Compressive Strength Results for Cubes

Aspect Ratio 60 Cubic Specimens				
Fiber Volume (%)	f_c	f_{st}	$f_{st}/f_{c\ cubes}$	$fc\ cyl/fc\ cu$
0.00	79.30	4.98	0.063	0.900
0.50	90.70	5.74	0.063	0.784
0.75	92.20	5.82	0.063	0.828
1.00	98.70	6.19	0.063	0.817
1.25	100.40	6.78	0.068	0.825
1.50	108.90	7.94	0.073	0.769
1.75	108.90	8.77	0.081	0.813
2.00	116.00	8.93	0.077	0.791
Aspect Ratio 75 Cubic Specimens				
Fiber Volume (%)	f_c	f_{st}	$f_{st}/f_{c\ cubes}$	$fc\ cyl/fc\ cu$
0.50	91.70	3.30	0.036	0.800
0.75	93.80	4.30	0.046	0.808
1.00	100.50	4.80	0.048	0.778
1.25	94.40	5.30	0.056	0.858
1.50	100.10	7.00	0.070	0.803
1.75	107.00	10.10	0.094	0.782
2.00	99.00	11.80	0.120	0.829

f_c = compressive strength; f_{st} = splitting tensile strength; f_{st}/f_c = splitting tensile strength to compressive strength; $f_c\ cyl/\ f_c\ cu$ = cylindrical compressive strength to cubic compressive strength ratio

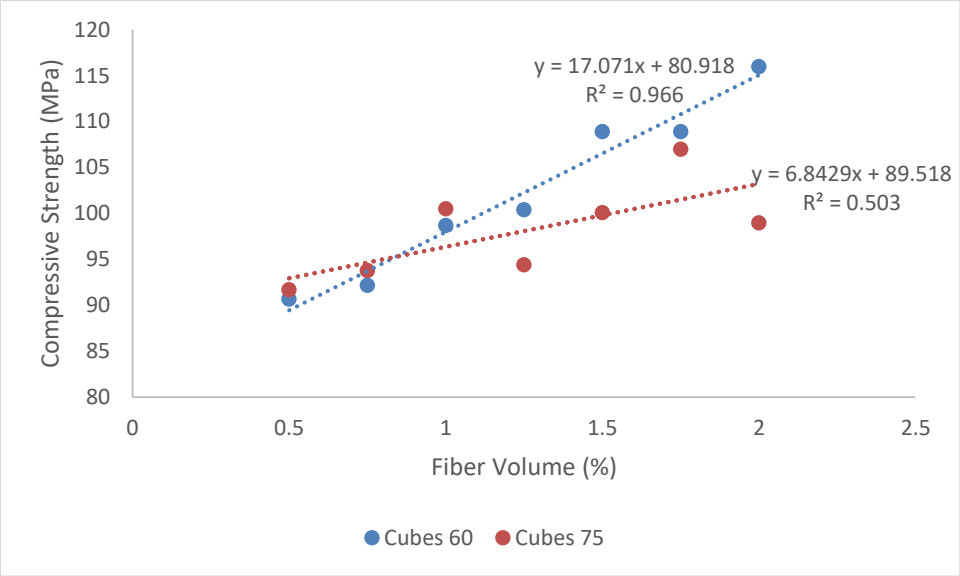

Fig-2: Relationship between cube compressive strength and fiber volume

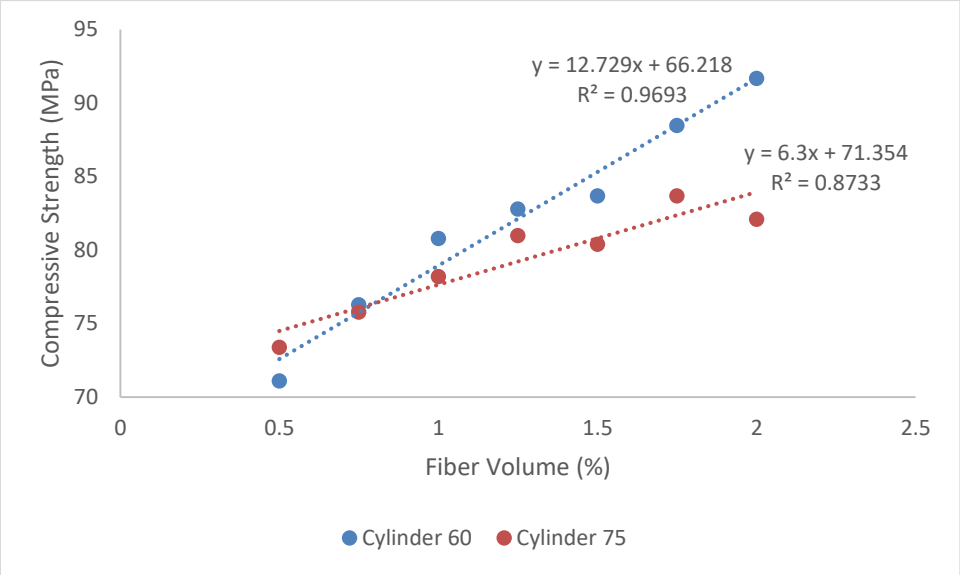

Fig-3: Relationship between cylinder compressive strength and fiber volume

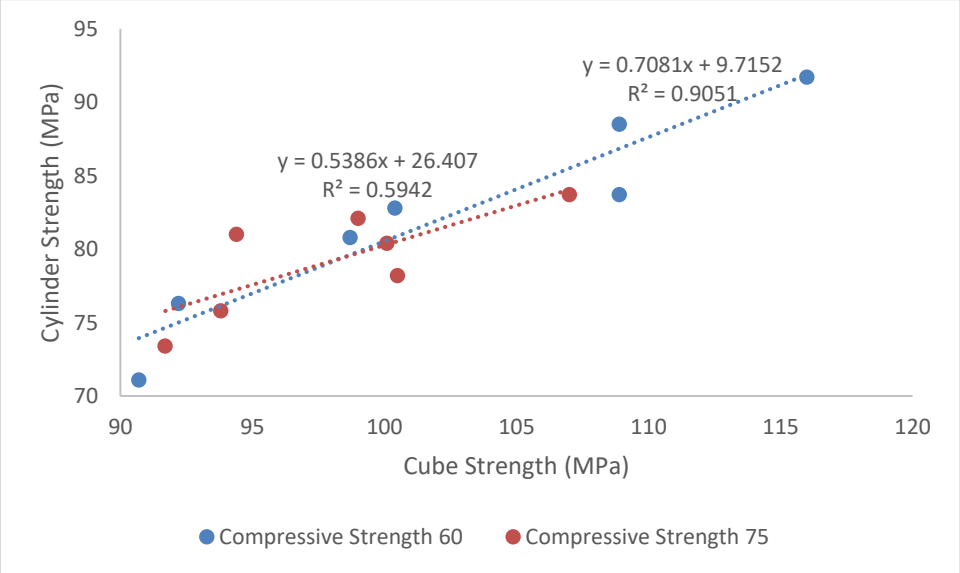

Fig-4: Relationship between cylinder strength and cube strength

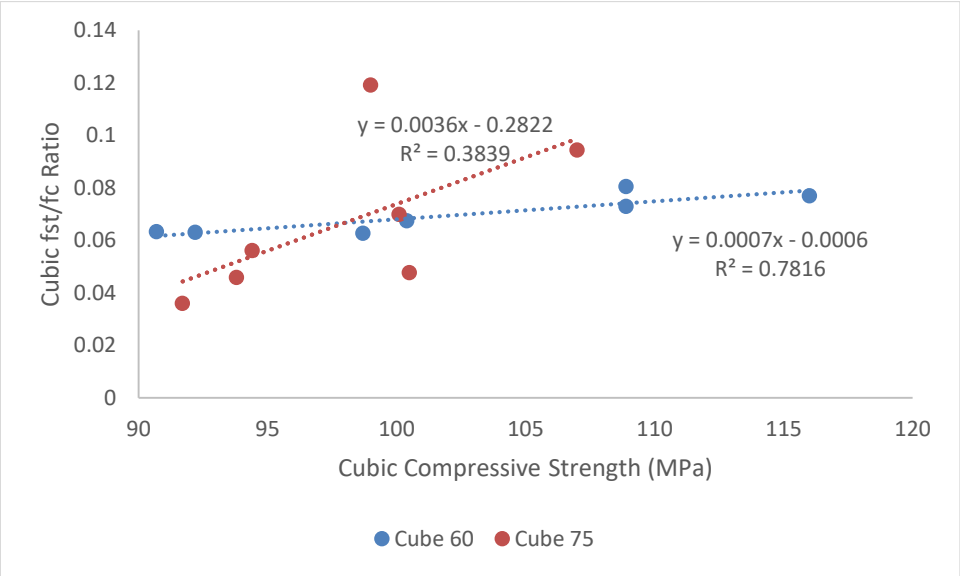

Fig-5: Splitting tensile strength vs compressive strength ratio

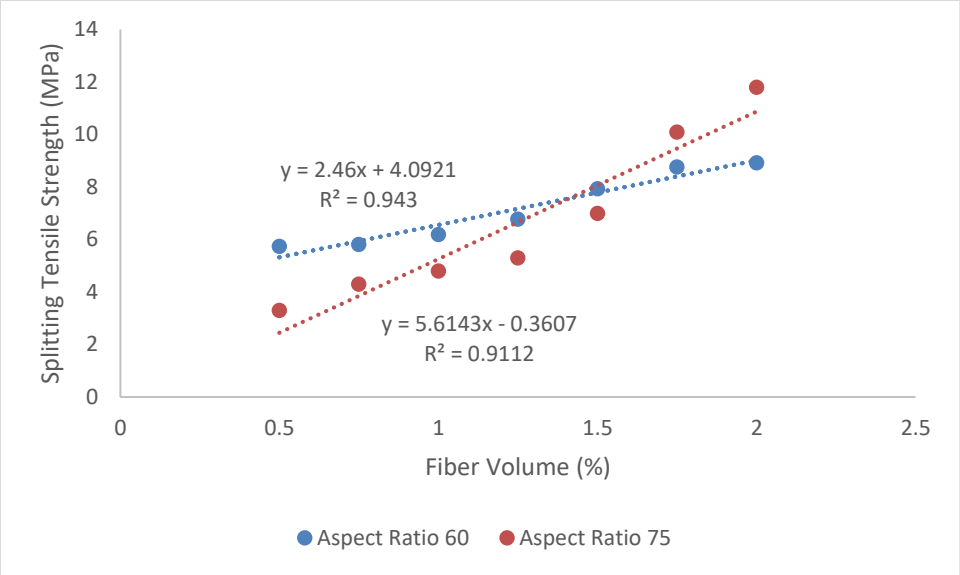

Fig-6: Relationship between splitting tensile strength and fiber volume

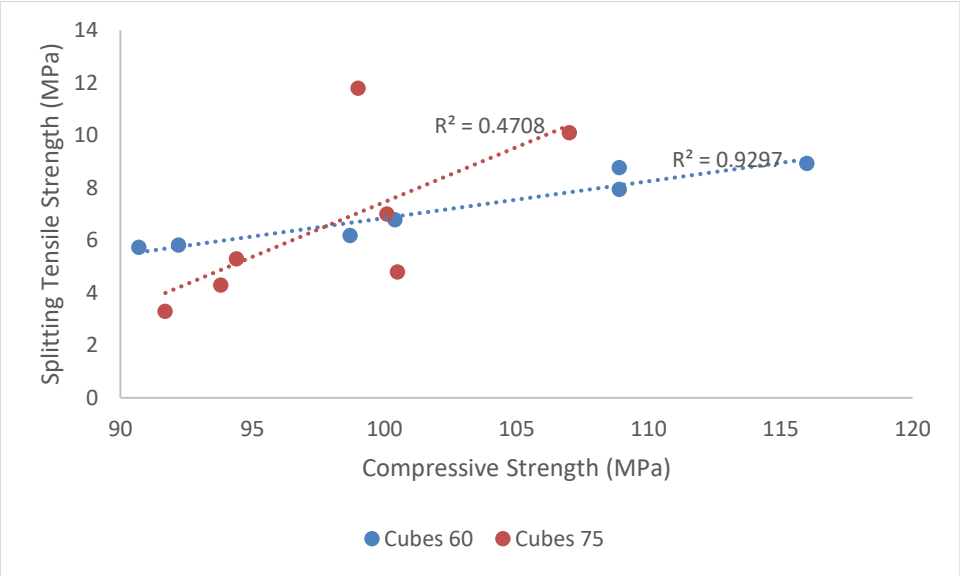

Fig-7: Relationship between splitting tensile strength and compressive strength for both cylinders and cubes

3.2 Statistical Evaluation

In Figures 8-11-10, a summary is presented of probability plots for mean of the set of data. The mean or average of each level with fiber addition is presented in the figures together with the standard deviation. Also depicted is the 5 % compressive strength based on a significance level of 0.05. Boxplot relationship depicting the spread of the values is presented in Figure 12-13. In aspect ratio 60 for cubes, the range is spread over a wide range of values, and the same trend was observed cylinders' aspect ratio 75. In cube 75, the median is very close to the third quartile (Q3), the same phenomenon was observed in cylinder 75, this is due to the fluctuations observed in the results at higher fiber dosage. This indicates the median of data is distributed in the upper portion of the graph. Boxplots generally display range and spread of values, as well as agreement or how different the range is. Additionally, it could be seen from Figure 11 that the Boxplots for the same type of specimen geometry (cube 60 & 75, and cylinder 60 & 75) met at some point in the graph, an indication of overlap that signifies the results have similar characteristics with the variation not that different.

The range or spread of the data increases or is wider in the lower aspect ratio, indicating some degree of variability compared with the higher aspect ratio. Standard error of the mean which shows the degree of variability of the sample mean presented in Table 4-5 indicated that 1.00% fiber addition had the highest error at 1.17. This is because the range of the samples is spread over a 5 MPa range as oppose to the others that had 2 – 3 MPa range. Standard deviation on the other hand which measured variability in the single sample showed a similar trend observed in standard error of mean. Variation in standard deviation will describe the range of the compressive strength as seen in Figures 8-11.

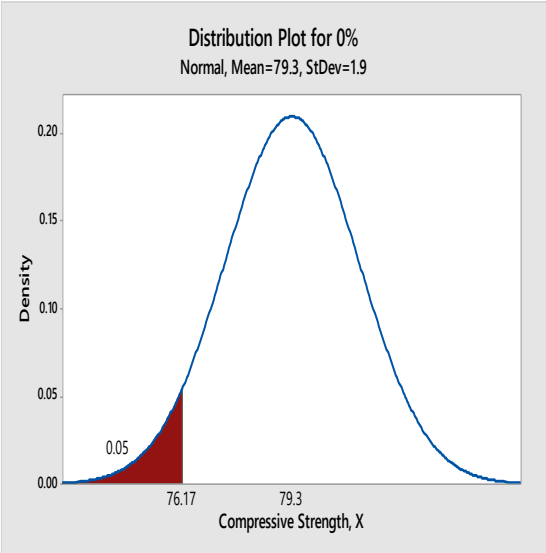
Distribution Plot for 0%
Normal, Mean=79.3, StDev=1.9
Density
0.20
0.15
0.10
0.05
0.00
0.05
76.17
79.3
Compressive Strength, X

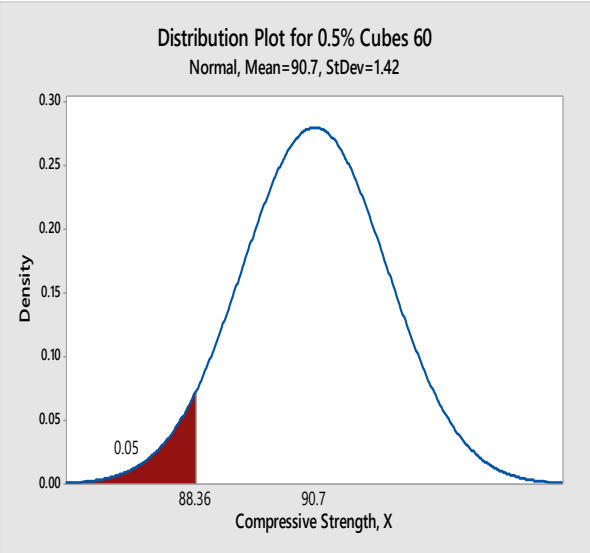
Distribution Plot for 0.5% Cubes 60
Normal, Mean=90.7, StDev=1.42
Density
0.30
0.25
0.20
0.15
0.10
0.05
0.00
0.05
88.36
90.7
Compressive Strength, X

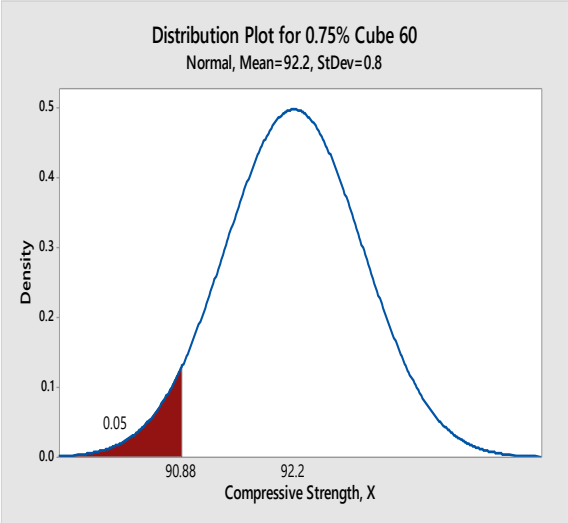
Distribution Plot for 0.75% Cube 60
Normal, Mean=92.2, StDev=0.8
Density
0.5
0.4
0.3
0.2
0.1
0.0
0.05
90.88
92.2
Compressive Strength, X

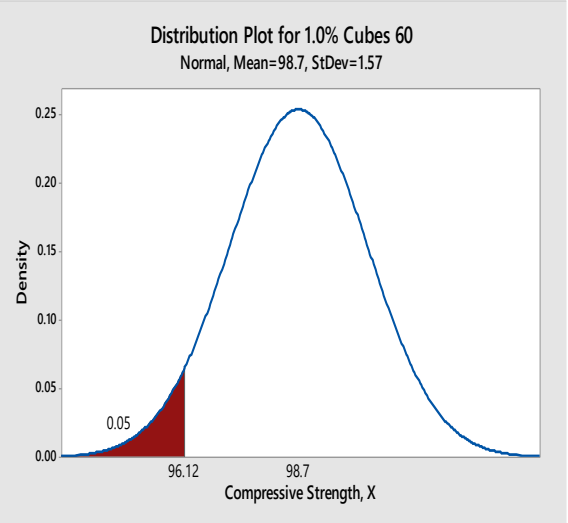
Distribution Plot for 1.0% Cubes 60
Normal, Mean=98.7, StDev=1.57
Density
0.25
0.20
0.15
0.10
0.05
0.00
0.05
96.12
98.7
Compressive Strength, X

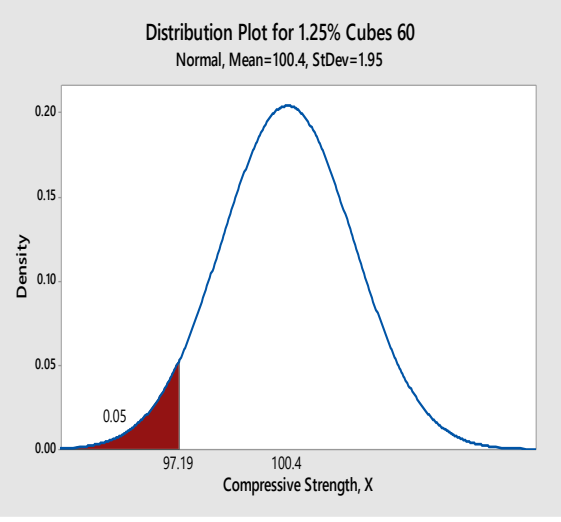
Distribution Plot for 1.25% Cubes 60
Normal, Mean=100.4, StDev=1.95
Density
0.20
0.15
0.10
0.05
0.00
0.05
97.19
100.4
Compressive Strength, X

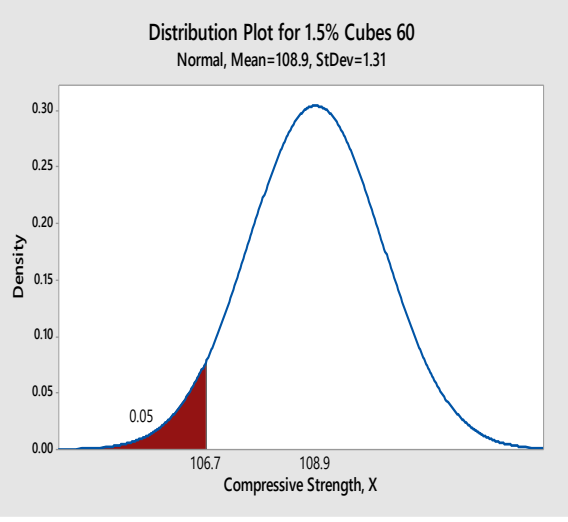
Distribution Plot for 1.5% Cubes 60
Normal, Mean=108.9, StDev=1.31
Density
0.30
0.25
0.20
0.15
0.10
0.05
0.00
0.05
106.7
108.9
Compressive Strength, X

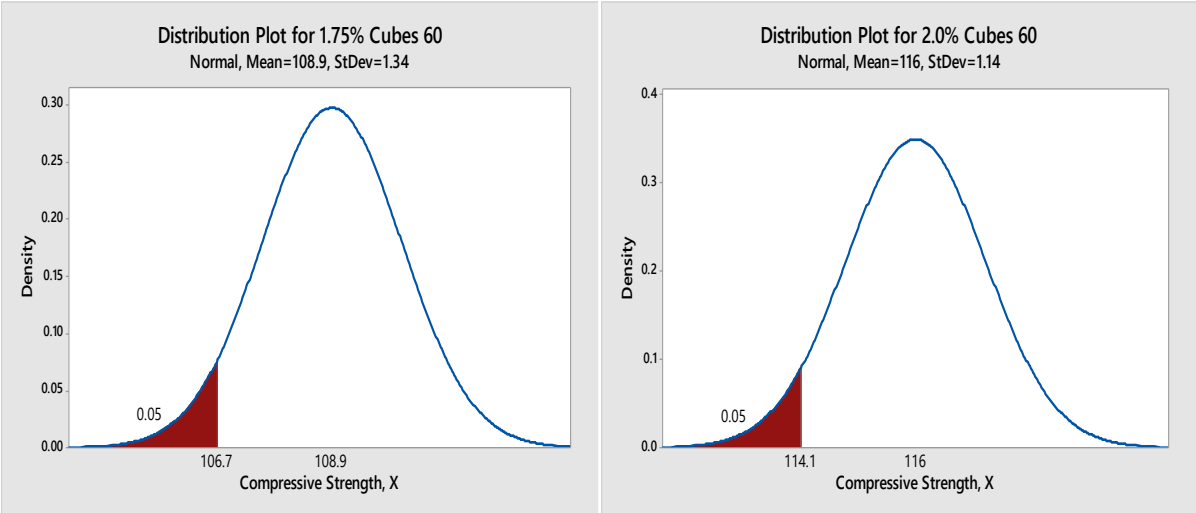

Fig-8: Probability plots for the mean results in cubes aspect ratio 60 with 5% of compressive strength results

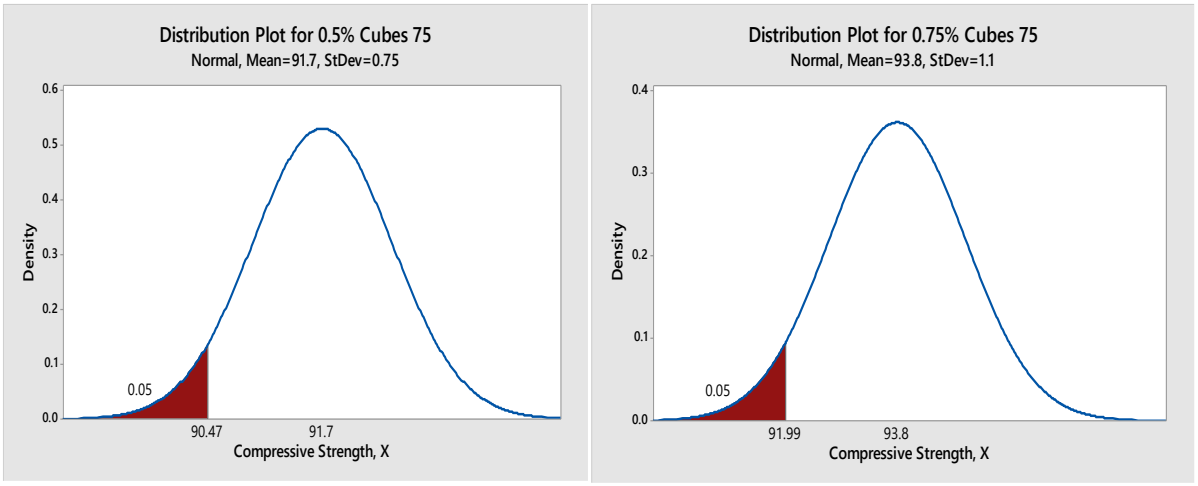

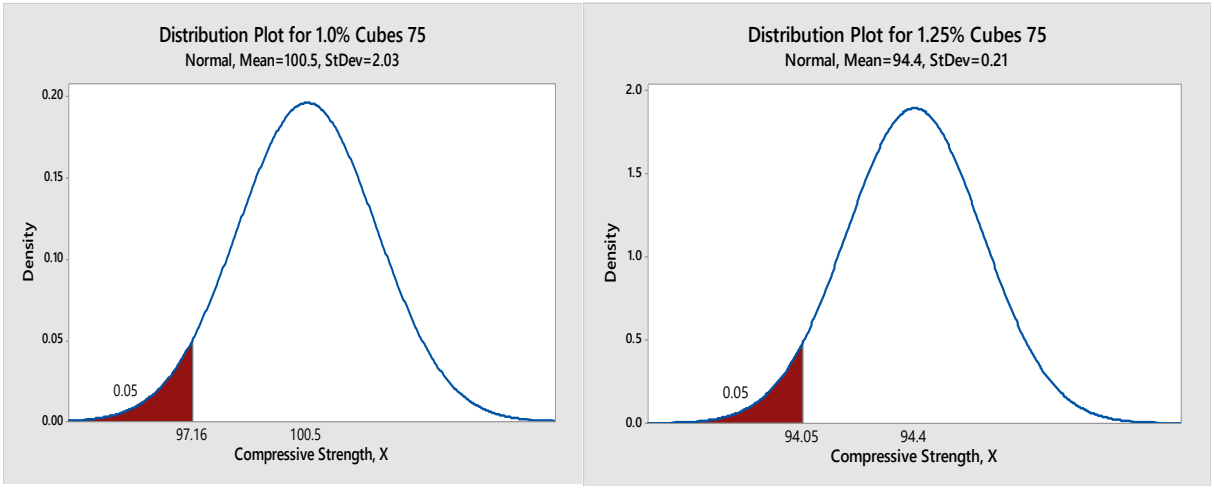

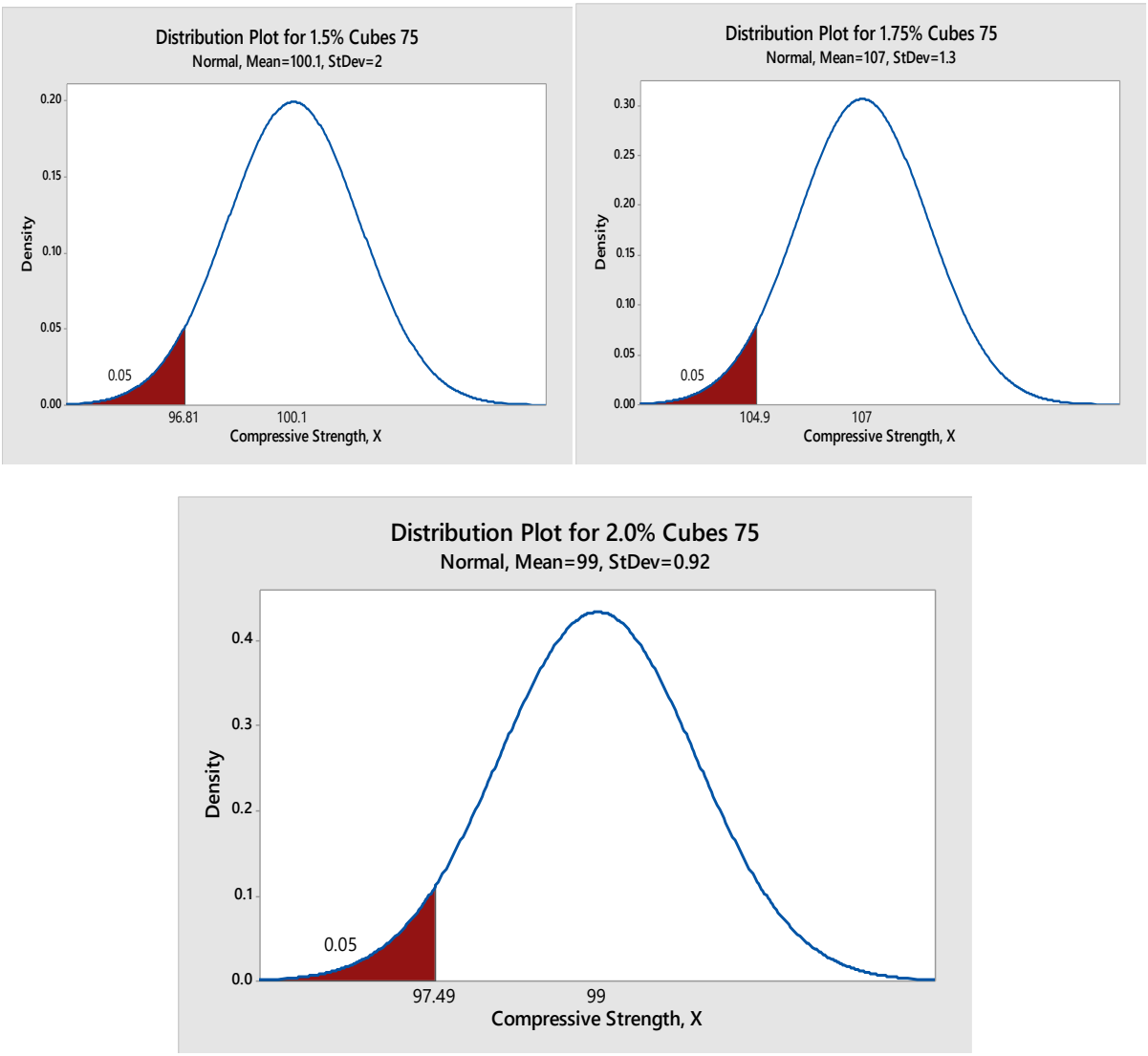

Fig-9: Probability plots for the mean results in cubes aspect ratio 75 with 5% of compressive strength results

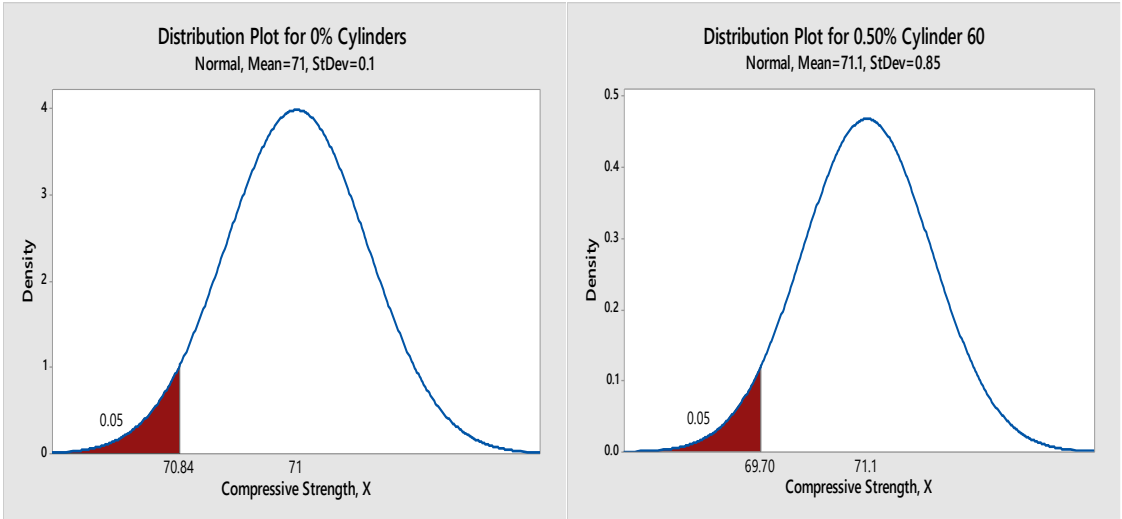

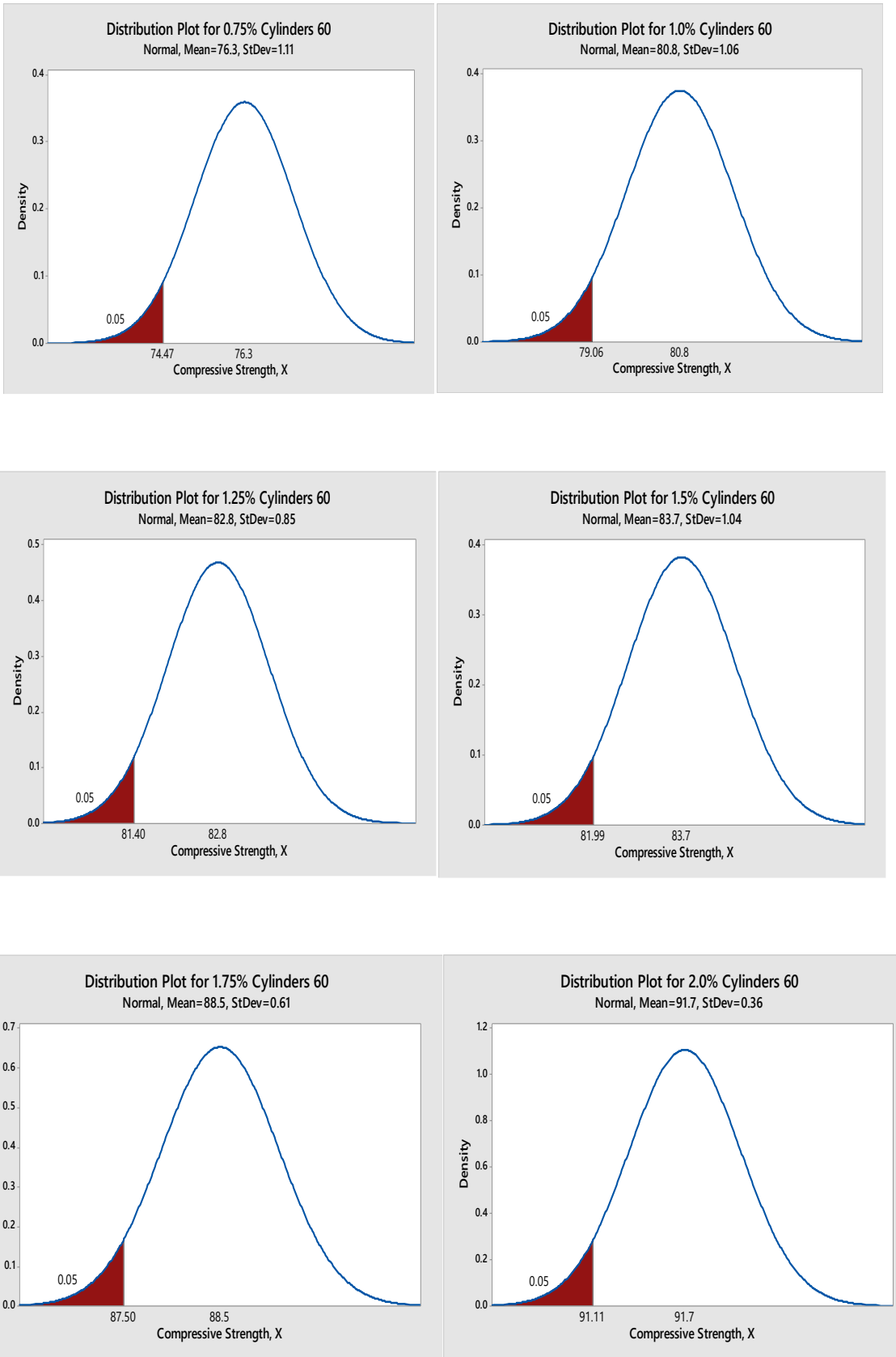

Fig-10: Probability plots for the mean results in cylinders' aspect ratio 60 with 5% of compressive strength results

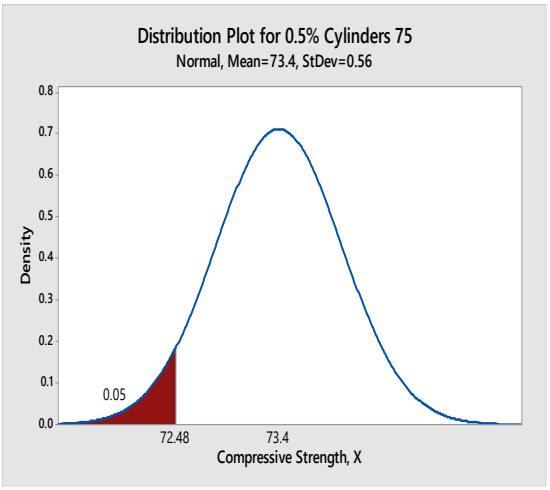
Distribution Plot for 0.5% Cylinders 75
Normal, Mean=73.4, StDev=0.56
Density
0.05
72.48
73.4
Compressive Strength, X

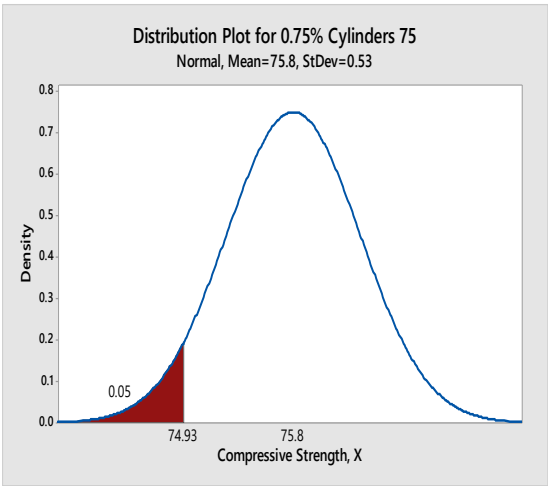
Distribution Plot for 0.75% Cylinders 75
Normal, Mean=75.8, StDev=0.53
Density
0.05
74.93
75.8
Compressive Strength, X

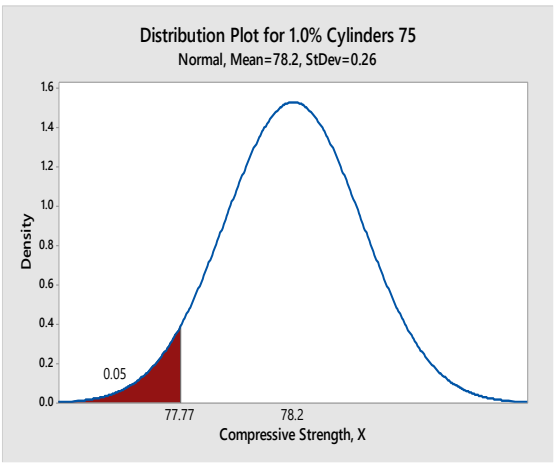
Distribution Plot for 1.0% Cylinders 75
Normal, Mean=78.2, StDev=0.26
Density
0.05
77.77
78.2
Compressive Strength, X

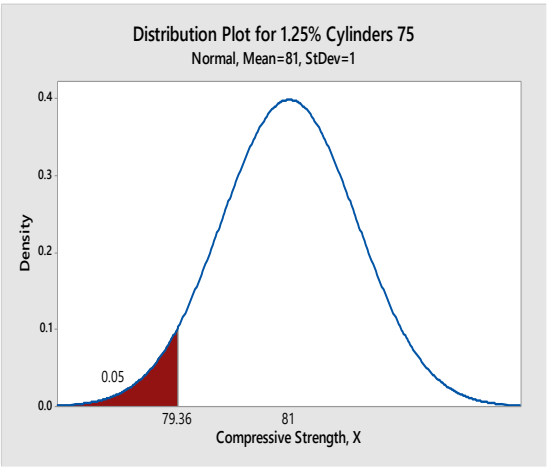
Distribution Plot for 1.25% Cylinders 75
Normal, Mean=81, StDev=1
Density
0.05
79.36
81
Compressive Strength, X

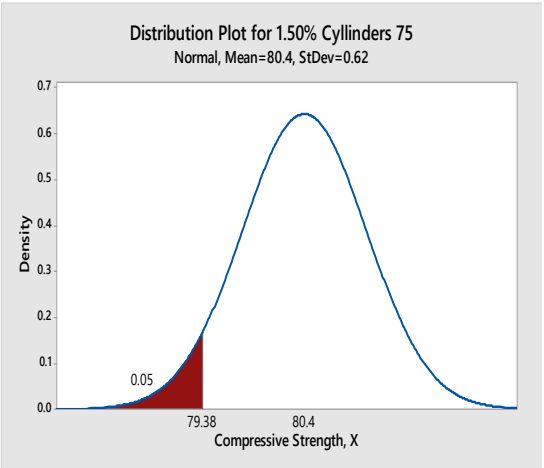
Distribution Plot for 1.50% Cyllinders 75
Normal, Mean=80.4, StDev=0.62
Density
0.05
79.38
80.4
Compressive Strength, X

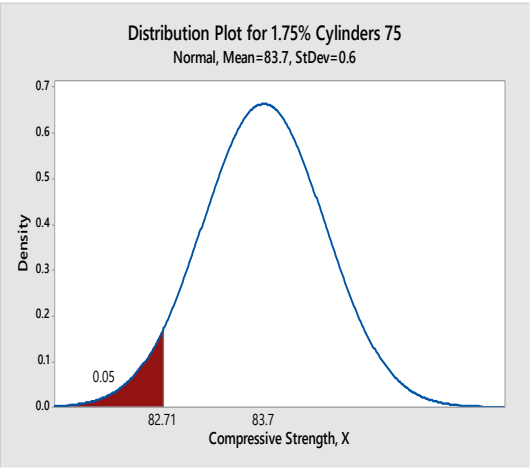
Distribution Plot for 1.75% Cylinders 75
Normal, Mean=83.7, StDev=0.6
Density
0.05
82.71
83.7
Compressive Strength, X

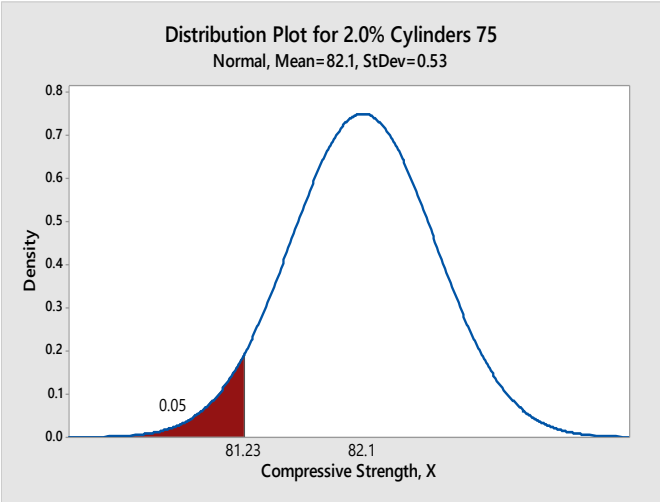

Fig-11: Probability plots for the mean results in cylinders' aspect ratio 75 with 5% of compressive strength results

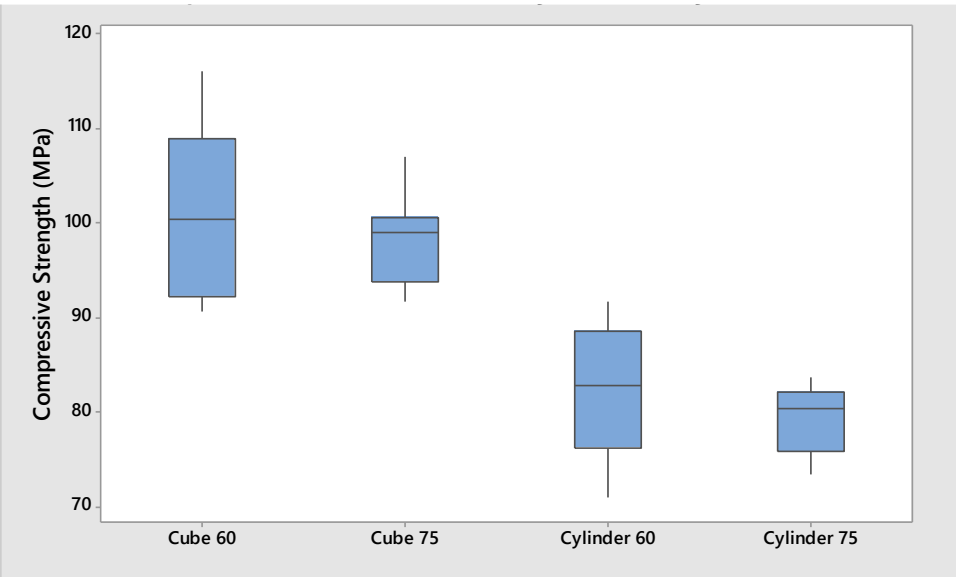

Fig-12: Boxplot relationships for compressive strength results of cubes and cylinders

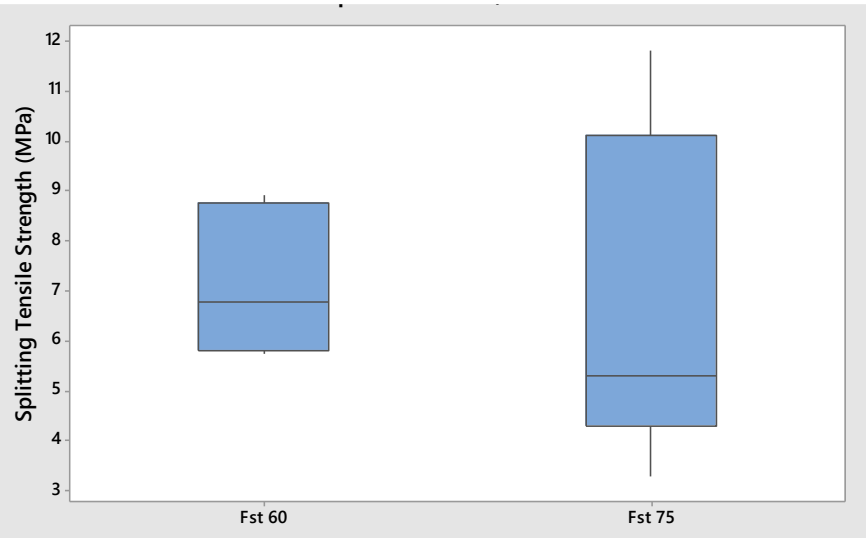

Fig-13: Boxplot relationships for splitting tensile strength results

4. CONCLUSION

In this study, an attempt has been made to investigate the variability of HPC with steel fiber addition using cylinders and cubes, and the following conclusions have been reached:

- An increase in compressive strength is observed for both prismatic and cylindrical specimens with fiber addition in aspect ratio 60, while the increment in aspect ratio 75 for both specimen geometry was up 1.00% addition. On the other hand, splitting tensile strength increase is observed in both aspect ratios, but more pronounced in l/d = 75 due to volume fraction increase.
- The ratio of the cylinder-to-cube specimen is within the range of 0.7 – 0.9. This is in line with suggested values for concrete above 50 MPa strength.
- Fiber addition resulted in 'wall effect' despite the fact that the maximum size of the aggregate is within the recommendation of the relevant standard. The wall effect is prominent in volume fraction in excess of 1.25% addition.
- Variability is more pronounced in lower aspect ratio of the fiber than in the higher aspect ratio because of the spread of the data set range.
- The range of the specimens utilized has been successfully reduced to within 2 – 3 MPa for the most part except in rare cases.

REFERENCES

[1] Neville, A.M. (2005), Properties of Concrete, 14th Ed. Wiley, New York

[2] Abubakar, A. U. (2018), "Influence of Steel Fiber Addition on Workability & Mechanical Behavior of High Performance Concrete", PhD Thesis, EMU, North Cyprus.

[3] Akcaoglu, T. (2003). Interfacial Transition Zone Behavior of Concrete by Means of a Single Coarse Aggregate Model, PhD Thesis, Eastern Mediterranean University, North Cyprus.

[4] Newman, K. (1965) "Criteria for the behavior of plain concrete under complex states of stress", Proc. Int. Conf. on the Structure of Concrete, London, Sept. 1965, pp. 255-274 (Cement and Concrete Association, London, 1968)

[5] Lea, F.M. (1960) "Cement Research: Retrospect and Prospect", Proc. 4th Int. Symposium on the Chemistry of Cement, Washington D.C., pp. 5-8
[6] Van Mier, J.G.M. (1984) "Strain-softening of concrete under multiaxial loading conditions", PhD Thesis, Eindhoven University of Technology, Eindhoven, The Netherlands
[7] del Viso, J.R., Carmona, J.R., Ruiz, G. (2008) "Shape and size effect on the compressive strength of high-strength concrete", Cement and Concrete Research. 38: 386-395
[8] Torretti, J.N., Benaija, E.H., Boulay, C. (1993) "Influence of boundary conditions on strain softening in concrete compression tests", Journal of Engineering Mechanics-ASCE 119 (12): 2369-2384
[9] Tam, C.T., Babu, D.S., Li, W. (2017) "EN 206 Conformity testing of concrete strength in compression" Procedia Engineering, 171:227-237
[10] Hamad, A.J. (2017) "Size and shape effect of specimen on the compressive strength of HPLWFC reinforced with glass fibers. Journal of King Saud University-Engineering Sciences, 29:373-380
[11] Nakbin, I.M., Dehestani, M., Beygi, M.H.A., Rezvani, M. (2014) "Effects of cube size placement direction on compressive strength of self-consolidating concrete", Construction and Building Materials, 59:144-150
[12] Juki, M.I., Awang, M., Mahamad, M.K.A., Boon, K.H., Othman, N., Abdul Kadir, A., Roslan, M.A., Khaled, F.S. (2013) "Relationship Between Compressive, Splitting Tensile and Flexural Strength of Concrete Containing Granulated Waste Polyethylene Terephthalate (PET) Bottles as Fine Aggregate" Advanced Materials Research, Vol. 795 pp. 356-359
[13] Tokyay, M., Ozdemir, M. (1997) "Specimen Shape and Size Effect on the Compressive Strength of Higher Strength Concrete", Cement and Concrete Research, 27(8):1281-1289
[14] Ferrara, L., Park, Y.D., Shah, S.P. (2008) "Correlation among fresh state behavior, fiber dispersion, and toughness properties of SFRCs". J Mater Civ Eng 20(7):493–501
[15] Barnett, S.J., Lataste, J.F., Parry, T., Millard, S.G., Soutsos, M.N. (2010) "Assessment of fibre orientation in ultra high performance fibre reinforced concrete and its effect on flexural strength". Mater Struct 43(7):1009–1023
[16] Soroushian, P. and Lee, C.D. (1990) "Distribution of Fibers in Steel Fiber Reinforced Concrete". ACI Materials Journal, Vol. 87, No. 5. Sept-Oct pp. 433-439
[17] Mansur, M.A., Chin, M.S., and Wee, T.H. (1999) "Stress-Strain Relationship of High-Strength Fiber Concrete in Compression", J.Mater. Civ. Eng. 11(1): 21-29
[18] Afroughsabet, V., Biolzi, L., Ozballaloglu, T. (2016), "High-performance fiber-reinforced concrete: a review". J.Mater. Sci. 51:6517-6551
[19] Ferrara, L, Ozyurt, N., Di Prisco, M. (2011) 'High mechanical performance of fibre reinforced cementitious composites: the role of ''casting-flow induced'' fibre orientation'. Mater Struct 44(1):109–128
[20] Grunewald, S. (2012) "Fibre reinforcement and the rheology of concrete". In: Roussel N (ed) Understanding the rheology of concrete. Woodhead Publishing Limited, Cambridge, pp 229–256
[21] Orbe. A., Cuadrado, J., Losada, R., Roji,´ E. (2012) "Framework for the design and analysis of steel fiber reinforced self-compacting concrete structures". Constr Build Mater 35:676–686
[22] Wille, K., Tue, N.V., Parra-Montesinos, G.J. (2014) "Fiber distribution and orientation in UHP-FRC beams and their effect on backward analysis". Mater Struct 47(11):1825–1838
[23] Aydin, E. (2017) "Staplewire-reinforced high-volume fly-ash cement paste composites". Constr. Build. Mater. 153: 393-401
[24] ASTM C595 (2017) Standard Specification for Blended Hydraulic Cements, ASTM International, West Conshohocken, PA, USA.

[25] BS EN 1008 (2002), Mixing water for concrete. Specification for sampling, testing and assessing the suitability of water, including water recovered from processes in the concrete industry, as mixing water for concrete, British Standard Institution, BSI London.
[26] ASTM C494 (2017) Standard Specification for Chemical Admixtures for Concrete, ASTM International, West Conshohocken, PA.
[27] ASTM C33 (2016) Standard Specification for Concrete Aggregates, ASTM International, West Conshohocken, PA
[28] ASTM C136 (2014) Standard Test Method for Sieve Analysis of Fine and Coarse Aggregates, ASTM International, West Conshohocken, PA
[29] ASTM C127 (2015) Standard Test Method for Relative Density (Specific Gravity) and Absorption of Coarse Aggregate, ASTM International, West Conshohocken, PA
[30] ASTM C128 (2015) Standard Test Method for Relative Density (Specific Gravity) and Absorption of Fine Aggregate, ASTM International, West Conshohocken, PA
[31] ASTM C29 (2017) Standard Test Method for Bulk Density ("Unit Weight") and Voids in Aggregate, ASTM International, West Conshohocken, PA.
[32] ASTM C117 (2013), Standard Test Method for Materials Finer than 75-µm (No 200) Sieve in Mineral Aggregates by Washing, ASTM International, West Conshohocken, PA.
[33] ASTM A820 (2011), Standard Specification for Steel Fibers for Fiber Reinforced Concrete, ASTM International, West Conshohocken, PA, USA.
[34] ASTM C39 (2018) Standard Test Method for Compressive Strength of Cylindrical Concrete Specimens, ASTM International, West Conshohocken, PA, USA.
[35] BS EN 12390-3: (2009), Testing hardened concrete. Compressive strength of test specimens, British Standard Institution, BSI London.
[36] BS EN 12390-6: (2009), Testing hardened concrete. Splitting Tensile Test of specimens, British Standard Institution, BSI London.
[37] Minitab 18 (2017), http://www.minitab.com/en-us/
[38] Edgington, J., Hannant, D.J. (1972) "Steel fibre reinforced concrete. The effect on fibre orientation of compaction by vibration". Mate´riaux et Construction 5(1):41–44
[39] Eren, O. and Celik, T. (1997) "Effect of silica fume and steel fibers on some properties of high-strength concrete". Constr. Build. Mater. Vol. 11 No. 7-8, pp. 373-382
[40] Evans, R.H. (1943) "The plastic theories for the ultimate strength of reinforced concrete beams", J. Inst. Civ. Engrs. 21, pp. 98-121
[41] CEP-FIP (1990) Model Code, Thomas Telford, London pp. 437
[42] ASTM C192 (2016). Standard Practice for Making and Curing Concrete Test Specimens in the Laboratory. ASTM International, West Conshohocken, PA, USA.